Atomistic simulations of grain coalescence

Andrew J. Detor
Lawrence Livermore National Laboratory, Materials Science and Technology Division, Livermore, California 94550, USA
(Received 17 July 2008; revised manuscript received 17 September 2008; published 31 October 2008)

Grain coalescence has been proposed as a mechanism for tensile stress generation in deposited films. The present work investigates this mechanism using atomistic simulations performed over a wide range of grain boundary configurations. Surface, grain boundary, and elastic strain energies are measured and correlated with the stress generated during coalescence. Strain accommodation at the atomic scale is shown to depend on the details of grain boundary structure, and the magnitude of stress developed is found to scale inversely with grain boundary energy. The results are compared with a popular continuum-level model that overestimates the maximum stress observed in the present simulations and also in experiments in the literature in general. It is concluded that grain coalescence is governed by the maximum range of atomic interaction across the coalescence gap, and the stress generated depends on the apparent stiffness of the coalescence reaction. These results have important implications in understanding the tensile stress developed in experiments and continuum-level models.

DOI: 10.1103/PhysRevB.78.144113 PACS number(s): 68.35.Gy, 68.35.Md, 68.55.A−

I. INTRODUCTION

The development of intrinsic stress in deposited films is an active area of research focused on controlling high stress levels that can lead to excessive deformation or complete failure of the film by cracking or spalling. Tensile stresses, in particular, have plagued a variety of materials and synthesis routes,[1–5] and strategies to reduce or eliminate these stresses require an understanding of the fundamental mechanisms of stress generation. While several theories have been proposed,[6] the most popular is based on grain coalescence as introduced in 1972 by Doljack and Hoffman.[7,8] This theory assumes that neighboring grains are attracted to one another under the action of interatomic forces leading to spontaneous coalescence and a net in-plane contraction of the film during deposition. Because the film is constrained by the substrate, this mechanism produces a tensile stress, σ, which can be approximated in the linear elastic region as[8]

$$\sigma = C\frac{\Delta}{d}, \tag{1}$$

where C is the material stiffness, Δ is the gap over which grains coalesce, and d is the grain size. The stiffness, C, is strictly a tensor quantity depending on the crystallographic orientation of coalescing grains; however, the biaxial modulus $E/(1-\nu)$, where E is Young's modulus and ν is Poisson's ratio, is typically substituted for C to provide an approximate measure of stress in polycrystalline films. The quantity Δ/d represents the strain developed in the system depending on the characteristic length scale of coalescence events. This relationship predicts that fine-grained films are exceedingly prone to tensile stress due to the high density of stress-generating grain boundaries. While stiffness and grain size are both straightforward to quantify, Δ in Eq. (1) continues to be the most elusive parameter. Several works have aimed at quantifying Δ based on either atomic bonding considerations[6–11] or global energetic analyses.[12] In the former, Δ is taken as the maximum range of atomic interaction calculated from interatomic potentials or approximated by atomic radii. The latter approach was introduced by Nix and Clemens,[12] who performed an energy balance between precoalescence and postcoalescence states similar in concept to the Griffith theory of fracture,[13] but in reverse (i.e., crack closing instead of opening). In their analysis, the initial, E_i, and final, E_f, energy states can be expressed as[12]

$$E_i = 2A\gamma_s, \tag{2}$$

$$E_f = A\gamma_{\mathrm{gb}} + E_{\mathrm{strain}}, \tag{3}$$

where A is the grain boundary area, γ_s and γ_{gb} are the surface and grain boundary energies, respectively, and $E_{\mathrm{strain}} = CA\Delta^2/2d$ is the elastic strain energy of coalescence. For cases where $E_i > E_f$, an elastically strained grain boundary is energetically favorable to two free surfaces and coalescence will occur. Solving for the critical condition $E_i = E_f$ gives an upper-bound estimate for the maximum possible coalescence gap, $\Delta_{\max}$;

$$\Delta_{\max} = \left[\frac{2d(2\gamma_s - \gamma_{\mathrm{gb}})}{C}\right]^{1/2}. \tag{4}$$

Inserting Eq. (4) into Eq. (1) leads to an expression that is one of the most commonly cited in reference to tensile stress development in deposited films;

$$\sigma_{\max} = \left[\frac{2C(2\gamma_s - \gamma_{\mathrm{gb}})}{d}\right]^{1/2}. \tag{5}$$

Originally derived by Nix and Clemens,[12] Eq. (5) has since spurred a number of works where researchers have extended the model to account for more complex geometries[14–16] and used these types of expressions in finite element calculations of grain coalescence.[17,18] All of these works implicitly contain the fundamental energy balance concept introduced above.

While previous studies have almost exclusively focused on continuum-level analyses, there has been very little effort approaching grain coalescence from an atomistic standpoint. The author is aware of only one recent work where atomistic

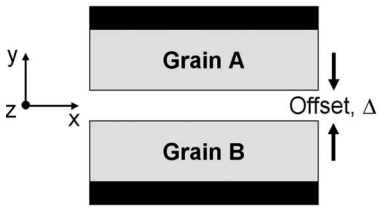

FIG. 1. Schematic of the simulation setup. Grains A and B are separated by an initial offset distance, Δ, and allowed to relax to a minimum energy state. Periodic boundary conditions are applied in the *x*-*z* plane, and atomic interactions are governed by a multibody potential for Ta. The stress developed upon relaxation is measured on the rigid (black) plates attached to each grain.

simulations were used to examine the coalescence of a single crystal,[19] but without incorporating grain boundaries the scaling of Eq. (5) could not be studied. Work is needed in this area as Eq. (5) typically overestimates experimental stresses[17,19–21] bringing to question the critical energy assumption upon which most studies are based. A better understanding of the grain coalescence mechanism should also lead to new techniques for reducing and controlling stress in experiments. A wide range of materials including, for example, Ta,[22] Ni,[23] Cr,[24,25] Cu,[26] Al,[11] Be,[27] Mo,[28,29] W,[30] and Au (Ref. 31) have all shown a tendency for high tensile stresses approaching a significant fraction of the yield strength, which is undesirable in most applications. The goal of the present work is to investigate grain coalescence through rigorous atomistic computer simulations over a wide range of grain boundary configurations. This approach enables direct observation of the mechanism and associated energetics of tensile stress generation. It also allows for quantitative comparison with analytical models to test the applicability of continuum-level approaches.

II. SIMULATION PROCEDURE

A schematic of the simulation setup is shown in Fig. 1. Two grains (A and B) are fixed between rigid plates, separated by an offset distance Δ. Both grains are constructed as body-centered cubic (bcc) with the [110] axis parallel to the *z* direction. Symmetric rotations about the [110] axis are performed to produce the 13 unique tilt grain boundaries listed in Table I, spanning a wide range of misorientation angles from 0 (i.e., single crystal) to 148.4°; the coincident site lattice (CSL) classification for each boundary is also listed. Periodic boundary conditions are applied in the *x*-*z* plane capturing the behavior of two infinite plates and eliminating complicated edge effects. For all simulations, dimensions in the *y* and *z* directions are set at 30 and 14 Å [6 (110) planes], respectively, for each grain, while the length in *x* depends on the periodic repeat distance of the particular structure under investigation, ranging from ~14–79 Å. The 30 Å dimension in *y* ensures that atoms in the grain boundary region are not influenced by the rigid plates, as will be seen in subsequent analyses. Atomic interactions are governed by an embedded-atom-method potential for Ta,[32] incorporating both first- and second-nearest-neighbor effects

TABLE I. Misorientation angle and CSL classification of all Ta [110] symmetric tilt boundaries studied in the present work.

Misorientation angle (deg)	CSL classification
0.0	Single crystal
3.4	Σ1153
6.7	Σ289
13.4	Σ73
20.0	Σ33
31.6	Σ27
38.9	Σ9
50.5	Σ11
59.0	Σ33
70.5	Σ3
109.5	Σ3
141.1	Σ9
148.4	Σ27

out to a radius of ~4 Å around each atom. This potential has been shown to accurately reproduce a number of properties in Ta including both surface energies and moduli.[32] Tantalum is chosen as a model material here, but the procedure and resulting trends should be applicable to transition metals in general.

Each simulation begins by applying a specified rigid offset Δ between grains A and B. Next, a molecular statics conjugate gradient relaxation routine is performed to minimize the energy of the system. Atoms are allowed to move off the original lattice of grains A and B in a direction dictated by the net local force; atoms in the rigid plates attached to A and B, however, remain fixed. For sufficiently small values of Δ, the free *x*-*z* surfaces of grains A and B are attracted and coalesce to form a grain boundary. Once the system energy is minimized, the average tensile stress produced by coalescence, σ, is measured on the fixed plates. Stress is calculated by summing the atomic-level forces in the *y* direction over each plate atom and normalizing by the simulated cell area in the *x*-*z* plane; in all cases the forces measured on the plates satisfy equilibrium conditions. It is important to note that the molecular statics routine implemented here captures only the enthalpy of coalescence. However, recent work has shown[19] that vibrational entropy effects are essentially negligible in the coalescence mechanism and hence are not expected to significantly affect the results presented here. It is also important to note that thermally activated relaxation mechanisms are not included in the present approach so that the stresses achieved represent an upper bound for the grain coalescence mechanism.

The simulations described above have been performed for a number of initial offset distances, Δ, for each of the grain boundaries listed in Table I. Comparing the energy, strain, and stress for each system allows for quantitative insight on the grain boundary coalescence mechanism.

III. ENERGETICS OF COALESCENCE

The driving force for coalescence, as proposed by Nix and Clemens,[12] is the elimination of two high-energy surfaces in

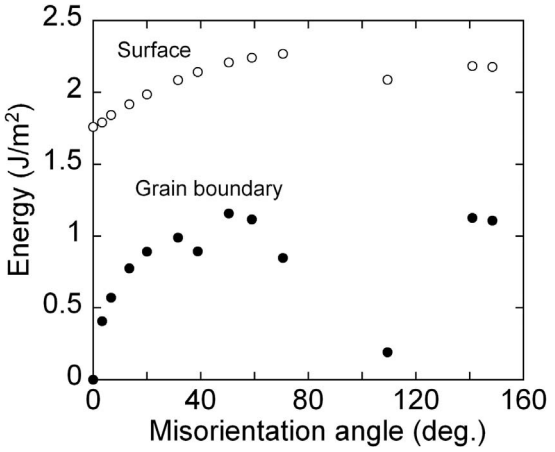

FIG. 2. Surface and grain boundary energies as functions of misorientation angle for the boundaries listed in Table I.

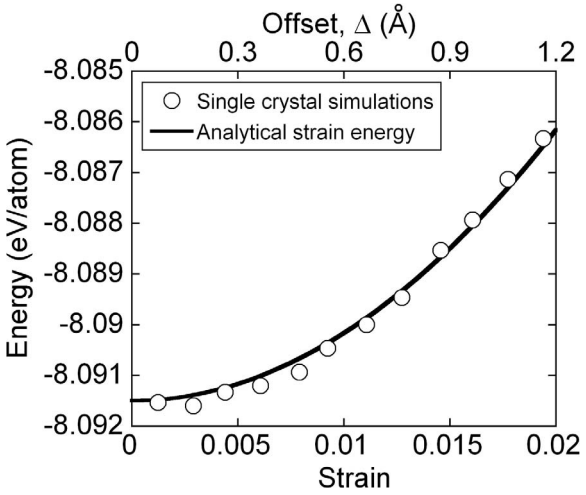

FIG. 3. Energy of the single-crystal simulations (open points) as a function of strain (offset) along with the linear elastic prediction, E_{strain} from Eq. (3), showing the elastic nature of the coalescence mechanism.

favor of a grain boundary. In the present work, atomistic simulations enable direct measurement of these defect energies, which will prove useful in comparing with analytical models. Grain boundary and surface energy for the 13 configurations listed in Table I are presented as a function of misorientation angle in Fig. 2. Both quantities are calculated by taking the difference in energy between a defective structure (including either a surface or grain boundary) in reference to that of an ideal single crystal and normalizing by area. For surface energy calculations, a large offset distance Δ was applied such that no interaction occurred between grains A and B, while grain boundary energy was calculated based on the minimum energy structure obtained over the entire range of offsets examined following the conjugate gradient relaxation routine. These minimum energy configurations are assigned a value of $\Delta=0$ in the present work and correspond to a state of zero normal stress on the boundary. The grain boundary energies reported in Fig. 2 therefore represent equilibrium values within the constraints of the present simulation technique. It is important to note that rigid displacements in the x or z directions, which have been shown to impact equilibrium energies and configurations in some cases,[33] have not been explored here. Nevertheless, the energy trends in Fig. 2 are generally consistent with those expected for [110] tilt boundaries[34–36] including the occurrence of low-energy cusps for "special" CSL boundaries. Most important for the present work, the simulated orientations span many different values of $2\gamma_s-\gamma_{\text{gb}}$ as required to test the scaling of existing grain boundary coalescence models [cf. Eq. (5)].

The energy difference between grain boundaries and surfaces revealed in Fig. 2 is an important factor for coalescence. However, the second term in Eq. (3), strain energy, also plays an important role. In order for coalescence to occur, the benefit of grain boundary formation (replacing $2\gamma_s$ with γ_{gb}) must outweigh the penalty from strain. To gain some understanding of the strain energy contribution, equilibrium energies for single-crystal simulations performed over a range of initial offsets, Δ, are plotted as open points in Fig. 3. Strain is quantified here as Δ/d, where $d=60$ Å is the effective grain size (i.e., the total length of the bicrystal in the y direction). It is important to note that the open points in Fig. 3 are *not* the result of a single tensile test but are each from unique coalescence simulations performed from different initial offset distances ranging from $\Delta\approx 0-1.2$ Å. These results are typical for all simulations performed in the present work; energy increases parabolically with strain consistent with the expected elastic analytical prediction, E_{strain} from Eq. (3), which is plotted as a solid line in Fig. 3. The stiffness, C, used in the analytical prediction was determined by performing a simulated tensile test on the single crystal yielding a value of 237 GPa, which is generally consistent with experimental measurements in Ta.[37] These results confirm that the coalescence mechanism can be described as an elastic process, and the addition of a strain energy term, E_{strain} in Eq. (3), adequately captures the energetics.

While global strain energy obeys the expected analytical prediction (Fig. 3), it is not clear how strain is accommodated on the atomic scale; these details are implicitly neglected in continuum-level models. To investigate this, atomic displacements occurring on coalescence are plotted in Figs. 4(a)–4(d) for several grain boundaries encompassing a range of energies and misorientation angles. All the boundaries shown here correspond to the final, equilibrium state after a macroscopic strain of 0.017 (i.e., initial offset distance of $\Delta=1$ Å). Note that only displacements in the y direction (which contribute to tensile coalescence stress) are quantified here; displacements in the x and z directions are relatively low in comparison. Several interesting observations can be made based on the results of Fig. 4. The low-energy $\Sigma 3$ boundary in (a) displays a smooth, monotonically decreasing displacement field from the grain boundary into the bulk. The higher-energy low-angle boundaries in (b) and (c), on the other hand, show discrete regions of highly localized atomic displacement corresponding to the positions of grain boundary dislocations. The displacement field around each dislocation is not necessarily symmetric here as it depends on the specific sequence of relaxation in the numerical conjugate gradient technique; i.e., atoms on one side of the grain

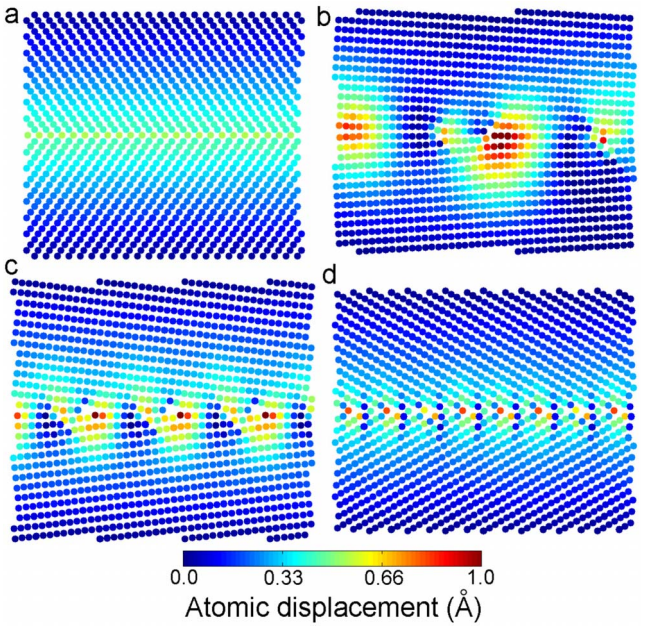

FIG. 4. (Color online) Atomic displacement (in the y direction) upon relaxation for the (a) 109.5° Σ3, (b) 6.7° Σ289, (c) 13.4° Σ73, and (d) 59.0° Σ33 boundaries arranged in order of increasing grain boundary energy. The macroscopic strain in all cases is 0.017 corresponding to an initial offset distance of $\Delta=1$ Å.

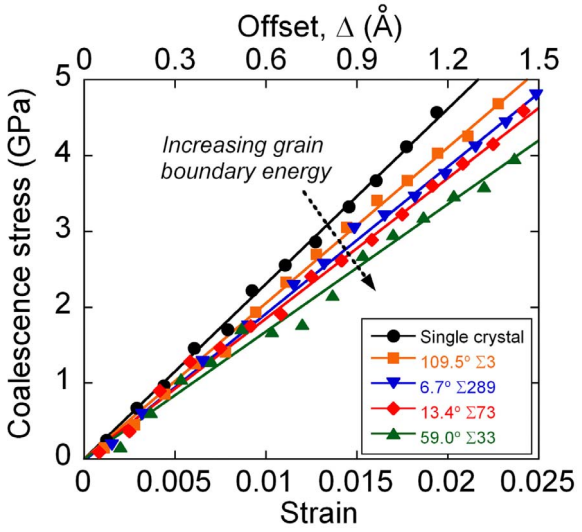

FIG. 5. (Color online) Average stress developed upon coalescence as a function of strain (offset). Elastic behavior is evident for all boundaries, but the apparent stiffness of coalescence decreases with increasing grain boundary energy.

boundary that initiate the relaxation process show slightly higher displacement. Nevertheless, the important point here is that displacement is localized in the vicinity of grain boundary dislocations. Lastly, the high-angle high-energy boundary in (d) displays somewhat mixed behavior with significant atomic-level displacement occurring in the immediate vicinity of the grain boundary and more uniform displacement extending into the bulk. The general features observed here can be rationalized based on grain boundary structure and the interactions occurring across the coalescence gap. For boundaries with low CSL classification [Fig. 4(a)] displacement is distributed uniformly due to the exceptional atomic registry between grains; random high-angle boundaries [Fig. 4(d)], on the other hand, exhibit localized displacement depending on the specific position of grain boundary atoms. For low-angle boundaries [Figs. 4(b) and 4(c)] that can be described as an array of dislocations, displacement is concentrated around these defects. In most experimental materials where grain boundaries are typically of general high-angle character, it is expected that the atomic-level displacement will be similar to that shown in Fig. 4(d). The various mechanisms of local strain accommodation will be shown to have important consequences on stress generation in Sec. IV.

An interesting point to note in passing pertains to the physical meaning of the offset distance Δ in the present work. In continuum approaches this variable is clearly interpreted as the distance between two perfectly flat surfaces. However, the atomic-scale definition of Δ depends on the local roughness at this length scale, as is apparent in Fig. 4, where slightly protruding or recessed atoms will experience different interaction distances across the grain boundary plane. For the purposes of the present work $\Delta=0$ has been defined as the rigid displacement between grains A and B that results in a minimum energy structure with zero normal stress acting on the boundary. Note, however, that this definition is merely for convenience and local effects ultimately dictate the strain developed across the coalescence gap as discussed above.

The results of Fig. 4 show how macroscopic strain is accommodated on the atomic scale during grain coalescence, and, from a global thermodynamic perspective, Fig. 3 demonstrates that the energy of this process is well described by an elastic calculation. In Sec. IV, the stress generated upon coalescence is examined and discussed in light of the energetic driving forces.

IV. TENSILE STRESS GENERATION

The stress-strain response of coalescence is plotted in Fig. 5 for boundaries with energy ranging from 0 (single crystal) to ~1.1 J/m^2. Linear elastic behavior is evident in all cases; however, there is a decrease in the apparent stiffness of coalescence with increasing grain boundary energy. It is again important to note that each data point in Fig. 5 is the result of a unique coalescence simulation for each boundary performed at an initial offset distance Δ and not from simulated tensile tests. The observed trend in stiffness is therefore related to the coalescence reaction. However, as mentioned in Sec. I, the anisotropy of stiffness in Ta (Refs. 37 and 38) must also be considered in evaluating this trend to rule out any possible contribution from different crystallographic orientations. Correcting for this effect, the apparent stiffness of coalescence for all boundaries investigated here is plotted in Fig. 6 relative to that expected for each orientation as a function of grain boundary energy. The single-crystal simulation at 0 J/m^2 displays the same stiffness in coalescence as expected in tension and thus has a relative value of zero. As

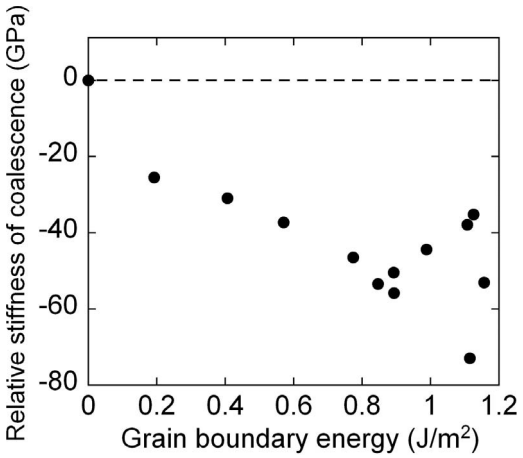

FIG. 6. Stiffness of the grain coalescence reaction relative to that expected for each grain boundary orientation (including anisotropic effects in Ta) as a function of grain boundary energy. Stiffness generally decreases as grain boundary energy increases.

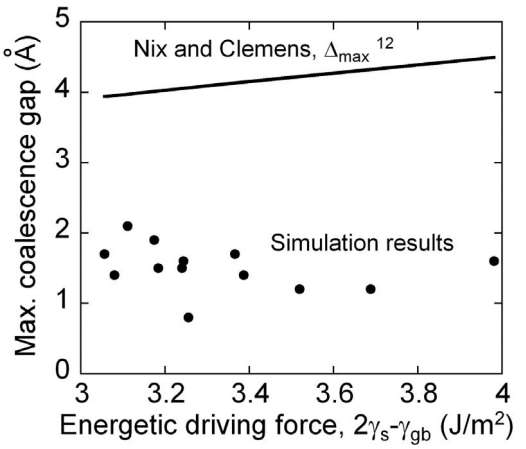

FIG. 7. Comparison of the maximum coalescence offsets observed in the present simulations with that predicted analytically by Nix and Clemens (Ref. 12). The analytical prediction, Δ_{max} from Eq. (4), overestimates the coalescence gap.

grain boundary energy increases, however, stiffness is found to generally decrease by as much as ~60 GPa below the expected value. The trend in stiffness is a direct consequence of the coalescence reaction, independent of orientation effects. This finding has significant implications for stress generation. For example, unlike the analysis leading to Eq. (5), low-energy boundaries may not necessarily generate higher stress as the result of a larger coalescence gap, Δ_{max} from Eq. (4). Instead, low-energy boundaries are inherently stiffer in coalescence generating higher stress levels at any given strain. A reasonable explanation may be that the *extent* of coalescence scales with the energetic driving force, $2\gamma_s - \gamma_{gb}$, leading to more complete coalescence in low-energy boundaries. This line of reasoning is qualitatively supported by the atomic strain data in Fig. 4, where the high-energy boundaries in (c) and (d) appear to contain relatively more free volume, suggesting that these structures have not coalesced completely. Although this interpretation differs from previous theories, it contains the same essential feature that stress scales with grain boundary energy. However, it brings into question the fundamental reason for this trend: is it based on the maximum achievable coalescence gap, Δ_{max}, or is it related to the extent of coalescence and the details of local strain accommodation in the boundary? This issue will be addressed in more detail in Sec. V.

V. COMPARISON WITH ANALYTICAL MODELS

The derivation of a maximum coalescence gap, Δ_{max} from Eq. (4), is a key component of the Nix and Clemens[12] energetic approach to coalescence stress. For a given material and grain size, this relationship predicts that Δ_{max} should increase with the driving force for coalescence $(2\gamma_s - \gamma_{gb})$. Both of these quantities are directly accessible in the present simulations, and values of Δ_{max} for each of the grain boundaries listed in Table I are plotted as a function of $2\gamma_s - \gamma_{gb}$ in Fig. 7; Δ_{max} is taken here as the critical offset beyond which no coalescence occurs in the simulations. Also plotted as a solid line in Fig. 7 is the analytical prediction of Eq. (4), which is found to overestimate the maximum coalescence gap by an average factor of 2 (ranging from 0.9 to as much as 4.1). The origin of this discrepancy can be understood by examining the inherent assumptions of the Nix and Clemens model in light of the present simulation results. Representative system energies from the single-crystal simulation are presented in Fig. 8 as a function of strain for both the initial (precoalescence) and final (postcoalescence/equilibrium) conditions plotted as open and closed points, respectively. Beyond a strain of ~0.02 (~1.2 Å offset), no coalescence occurs in the single crystal, and hence no solid points are plotted. Note that the initial energy plateaus at this same

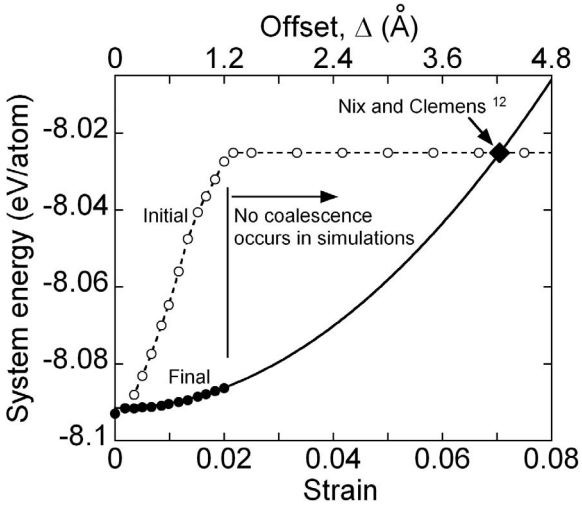

FIG. 8. Initial and final (equilibrium) system energies for the single-crystal simulations plotted as open and closed points, respectively; no coalescence occurs beyond a strain level of ~0.02 (1.2 Å offset). The energetic analysis of Nix and Clemens is demonstrated by extrapolating the final elastic strain energy to the point of intersection with the initial energy. The condition for grain coalescence is apparently governed by the maximum length scale of atomic interactions rather than the global energetics of the system.

limit, indicating that the free surfaces of grains A and B are no longer interacting. Also plotted as a solid line in Fig. 8 is the elastic prediction for final system energy from Fig. 3 extrapolated well beyond the maximum coalescence strain observed in simulations. The prediction of Nix and Clemens [Eq. (4)] is shown by a solid diamond at the intersection of the initial and final energy curves where the critical condition $E_i = E_f$ is satisfied. From this construction it is clear that the maximum coalescence strain from Eq. (4) greatly overestimates the fundamental limit set by the length scale of atomic interactions. Although the system energy could be lowered by coalescence, there is no interaction across the coalescence gap to initiate the process. As mentioned in Sec. I, a number of works have approximated $\Delta_{\max}$ based on atomic bonding considerations[6–11] instead of the global thermodynamics of the system, which appears here to be the more appropriate method. For example, several authors[6,9,11] have used the relationship;

$$\Delta_{\max} = \frac{a\phi - \phi^2/2}{2a - \phi} \approx r_o, \tag{6}$$

where a is the lattice parameter and $\phi \approx 2r_o$ is the distance of closest approach between atoms, typically approximated by the ionic diameter ($2r_o$). This expression agrees reasonably well with the simulation results of Fig. 7 where r_o for Ta is ~ 0.7 Å.[39] The energetic Griffith-type approach, on the other hand, is only valid under the constraint that atomic interactions actually occur across the coalescence gap. While it may be argued that this global energetic analysis could be recovered by simply extending the range of the interatomic potential, it is unlikely that sufficient interaction occurs over the required offset distance of ~ 4 Å. It is also important to again point out the accuracy of the current potential in reproducing numerous properties in Ta,[32] including those sensitive to longer-range interactions. Furthermore, the coalescence simulations performed by Seel *et al.*[19] mentioned in Sec. I included an interatomic potential extending to 15 Å, and the authors found that coalescence still only occurred over distances of $\sim 1-3$ Å, well in line with the present work. The results of Figs. 7 and 8 are therefore expected to accurately represent Ta bonding, suggesting that coalescence is limited by the maximum range of atomic interaction rather than global energetic considerations. Consequently, the tensile stress developed in deposited materials should not scale with the energetic driving force ($2\gamma_s - \gamma_{gb}$) via Eqs. (4) and (5). Although the formation of a grain boundary (in lieu of two free surfaces) is still ultimately the energetic rationale for coalescence, the limiting maximum offset distance is more appropriately calculated based on atomic bonding using Eq. (6), for example. This limiting condition should be incorporated into the various analytical models and finite element calculations referenced in Sec. I[14–18] that have relied on a global energetic approach to determine the length scale where opposing grains coalesce. Future work should also be directed at the stiffness relationship revealed in Fig. 6, including more detailed atomistic simulations and incorporation of stiffness dependence in continuum-level models.

VI. CONCLUSIONS AND IMPLICATIONS

Atomistic simulations have been used in the present work to investigate grain coalescence, a mechanism for tensile stress generation in deposited films. A variety of tilt grain boundary configurations have been studied, enabling comparisons over a wide range of misorientation angles and energies. The main conclusions of this work may be summarized as follows:

(i) Grain coalescence is elastic from a continuum perspective, although details of the atomic-level strain depend on the specific nature of the grain boundary; whether of low or high angle or of special low-index CSL classification.

(ii) Coalescence is limited by the maximum range of atomic interactions rather than the global energetics of the system as assumed in most models to date.

(iii) Grain boundary structure affects the stiffness of the coalescence reaction with low-energy boundaries displaying stiffer response (thus generating higher stresses). This finding is explained based on the extent of coalescence and local strain accommodation at the boundary.

The conclusions outlined above have important implications for both analytical modeling efforts and experiments. For example, the maximum coalescence gap (and stress) predicted using a popular analytical model was found to overestimate that observed in simulations by a factor of ~ 2 (cf. Sec. V). Although the coalescence reaction may be energetically feasible at large offsets, it was shown that the length scale required to initiate the process is greater than that reasonably achieved at the atomic level. The tensile stress generated in experiments should therefore more adequately be described by Eq. (1) with Δ based on atomic bonding considerations [cf. Eq. (6)]. Also, the concept of stiffness in the coalescence reaction has not been discussed previously, and the trend found here suggests that low-energy boundaries will lead to higher tensile stresses due to a stiffer response. This interpretation is in contrast to the traditional view where high stresses are caused by large coalescence gaps based on global energetic considerations. Coalescence stiffness and its dependence on grain boundary structure should be explored in future continuum and atomistic approaches to better understand tensile stress generation in deposited films.

ACKNOWLEDGMENTS

This work was performed under the auspices of the U.S. Department of Energy by Lawrence Livermore National Laboratory under Contract No. DE-AC52-07NA27344. The author thanks Megan Frary, Jason Trelewicz, and Morris Wang for useful discussions.

[1] J. W. Dini, *Electrodeposition: The Materials Science of Coatings and Substrates* (Noyes, Westwood, NJ, 1993).
[2] M. Ignat, in *Chemical Vapor Deposition*, edited by J.-H. Park and T. S. Sudarshan (ASM International, Materials Park, OH, 2001).
[3] D. M. Mattox, *Handbook of Physical Vapor Deposition (PVD) Processing* (Noyes, Westwood, NJ, 1998).
[4] M. Ohring, *Materials Science of Thin Films: Deposition and Structure* (Academic, Boston, MA, 2002).
[5] T. Watanabe, *Nano-Plating: Microstructure Control Theory of Plated Film and Data Base of Plated Film Microstructure* (Elsevier, Boston, MA, 2004).
[6] H. Windischmann, Crit. Rev. Solid State Mater. Sci. **17**, 547 (1992).
[7] F. A. Doljack and R. W. Hoffman, Thin Solid Films **12**, 71 (1972).
[8] R. W. Hoffman, Thin Solid Films **34**, 185 (1976).
[9] H. K. Pulker, Thin Solid Films **89**, 191 (1982).
[10] H. K. Pulker and J. Maser, Thin Solid Films **59**, 65 (1979).
[11] S. P. Kim, H. M. Choi, and S. K. Choi, Thin Solid Films **322**, 298 (1998).
[12] W. D. Nix and B. M. Clemens, J. Mater. Res. **14**, 3467 (1999).
[13] T. H. Courtney, *Mechanical Behavior of Materials* (McGraw-Hill, Boston, MA, 2000).
[14] L. B. Freund and E. Chason, J. Appl. Phys. **89**, 4866 (2001).
[15] B. W. Sheldon, K. H. A. Lau, and A. Rajamani, J. Appl. Phys. **90**, 5097 (2001).
[16] B. W. Sheldon, A. Bhandari, A. F. Bower, S. Raghavan, X. Wend, and J. M. Redwing, Acta Mater. **55**, 4973 (2007).
[17] S. C. Seel, C. V. Thompson, S. J. Hearne, and J. A. Floro, J. Appl. Phys. **88**, 7079 (2000).
[18] S. C. Seel and C. V. Thompson, J. Appl. Phys. **93**, 9038 (2003).
[19] S. C. Seel, J. J. Hoyt, E. B. Webb, and J. A. Zimmerman, Phys. Rev. B **73**, 245402 (2006).
[20] J. A. Floro, S. J. Hearne, J. A. Hunter, P. Kotula, E. Chason, S. C. Seel, and C. V. Thompson, J. Appl. Phys. **89**, 4886 (2001).
[21] S. J. Hearne, J. A. Floro, M. A. Rodriguez, R. T. Tissot, C. S. Frazer, L. Brewer, P. Hlava, and S. Foiles, J. Appl. Phys. **99**, 053517 (2006).
[22] B. L. French and J. C. Bilello, Thin Solid Films **446**, 91 (2004).
[23] J. A. Alfonso, E. D. Greaves, B. Lavelle, and L. Sajo-Bohus, J. Vac. Sci. Technol. B **21**, 846 (2003).
[24] A. Misra and M. Nastasi, J. Mater. Res. **14**, 4466 (1999).
[25] G. C. A. M. Janssen and J. D. Kamminga, Appl. Phys. Lett. **85**, 3086 (2004).
[26] H. M. Choi, S. K. Choi, O. Anderson, and K. Bange, Thin Solid Films **358**, 202 (2000).
[27] A. J. Detor, A. M. Hodge, E. Chason, M. Wang, H. Xu, M. Conyers, A. Nikroo, and A. Hamza (unpublished).
[28] Y. G. Shen, Mater. Sci. Eng., A **359**, 158 (2003).
[29] M. Andritschky and V. Teixeira, Vacuum **43**, 455 (1992).
[30] Y. G. Shen, Y. W. Mai, Q. C. Zhang, D. R. McKenzie, W. D. McFall, and W. E. McBride, J. Appl. Phys. **87**, 177 (2000).
[31] W. Tang, K. W. Xu, P. Wang, and M. Li, Mater. Lett. **57**, 3101 (2003).
[32] Y. H. Li, D. J. Siegel, J. B. Adams, and X. Y. Liu, Phys. Rev. B **67**, 125101 (2003).
[33] D. Yesilleten and T. A. Arias, Phys. Rev. B **64**, 174101 (2001).
[34] D. Wolf, Philos. Mag. A **62**, 447 (1990).
[35] R. Watanabe, A. Nogami, and T. Matsumiya, Mater. Sci. Forum **204-206**, 227 (1996).
[36] S. Tsurekawa, T. Tanaka, and H. Yoshinaga, Mater. Sci. Eng., A **176**, 341 (1994).
[37] F. H. Featherston and J. R. Neighbours, Phys. Rev. **130**, 1324 (1963).
[38] R. G. Leisure, D. K. Hsu, and B. A. Seiber, J. Appl. Phys. **44**, 3394 (1973).
[39] *CRC Handbook of Chemistry and Physics*, edited by D. R. Lide (CRC, Boca Raton, FL, 2000), Vol. 81.